

Epigenomic analysis of Alzheimer's disease brains reveals diminished CTCF binding on genes involved in synaptic organization

Prachetas J. Patel, Yong Ren, Zhen Yan*

Department of Physiology and Biophysics, State University of New York at Buffalo, Jacobs School of Medicine and Biomedical Sciences, Buffalo, NY 14203, USA

ARTICLE INFO

Keywords:

Alzheimer's disease
Epigenetics
CTCF
Chromatin organization
Synaptic genes
Histone acetylation

ABSTRACT

Epigenetic aberrations are suggested to play an important role in transcriptional alterations in Alzheimer's disease (AD). One of the key mechanisms of epigenetic regulation of gene expression is through the dynamic organization of chromatin structure via the master genome architecture protein, CCCTC-binding factor (CTCF). By forming chromatin loops, CTCF can influence gene transcription in a complex manner. To find out whether genome-wide DNA binding sites for CTCF are altered in AD, we compared CTCF chromatin immunoprecipitation sequencing (ChIP-Seq) data from frontal cortex of human AD patients and normal controls ($n = 9$ pairs, all females). We have revealed that CTCF-binding affinity on many genes is significantly reduced in AD patients, and these genes are enriched in synaptic organization, cell adhesion, and actin cytoskeleton, including synaptic scaffolding molecules and receptors, such as *SHANK2*, *HOMER1*, *NRXN1*, *CNTNAP2* and *GRIN2A*, and proto-cadherin (*PCDH*) and cadherin (*CDH*) family members. By comparing transcriptomic data from AD patients, we have discovered that many of the synaptic and adhesion genes with reduced CTCF binding in AD are significantly reduced in their mRNA expression. Moreover, a significant overlap of genes with the diminished CTCF binding and the reduced H3K27ac is identified in AD, with the common genes enriched in synaptic organization. These data suggest that the CTCF-controlled 3D chromatin organization is perturbed in AD, which may be linked to the diminished expression of target genes, probably through changes in histone modification.

1. Introduction

Alzheimer's disease (AD) is a complex neurodegenerative disorder with multiple pathological features, including synapse loss, synaptic and neuronal network dysfunction (Selkoe, 2002; Tracy and Gan, 2018; Wilson 3rd et al., 2023). Large-scale transcriptomic studies have revealed numerous genes with altered expression in postmortem prefrontal cortex (PFC) of AD patients (Mathys et al., 2019; Zhang et al., 2013). However, it is unclear how the aberrations in gene transcription occur in AD.

Epigenetic control, which largely involves chromatin remodeling, is a key avenue to achieve transcriptional regulation of gene expression in neurons (Borrelli et al., 2008). Epigenetic alterations are found to be a primary hallmark and causal driver of aging (López-Otín et al., 2023; Yang et al., 2023), the most prominent contributing factor of AD. Mammalian genomes are packaged into hierarchical levels, including active and inactive chromatin compartments at the mega-base scale and topologically associating domains (TADs) at the sub-megabase scale (Dixon et al., 2012; Lieberman-Aiden et al., 2009). Genomic function is

significantly influenced by chromatin organization in the three-dimensional nuclear space (Fraser and Bickmore, 2007; Lanctôt et al., 2007). The multifunctional zinc finger protein, CCCTC-binding factor (CTCF), is identified as a master organizer of chromatin architecture, which plays an essential role in mediating intra- and inter-chromosomal contacts (Merkenschlager and Duncan, 2013; Ong and Corces, 2014; Phillips and Corces, 2009). CTCF binds to a wide range of variant sequences to form genome-wide chromatin loops (Nora et al., 2017; Rao et al., 2014), coordinating long-range interactions between regulatory elements to control gene expression (Dehingia et al., 2022; Kubo et al., 2021; Merkenschlager and Odom, 2013; Ohlsson et al., 2010; Phillips and Corces, 2009).

De novo mutations in CTCF have been associated with various diseases, including Intellectual Disability, Schizophrenia, and cancer (Dehingia et al., 2022; Konrad et al., 2019; Ohlsson et al., 2001). Previous in vitro studies found that CTCF bound with a high affinity at the promoter region of Amyloid β -Protein Precursor, serving as a transcriptional activator (Vostrov and Quitschke, 1997). Here we examined whether CTCF occupancy was altered in AD brains. By bioinformatic

* Corresponding author.

E-mail address: zhenyan@buffalo.edu (Z. Yan).

<https://doi.org/10.1016/j.nbd.2023.106192>

Received 6 February 2023; Received in revised form 31 May 2023; Accepted 1 June 2023

Available online 10 June 2023

0969-9961/© 2023 The Authors. Published by Elsevier Inc. This is an open access article under the CC BY-NC-ND license (<http://creativecommons.org/licenses/by-nc-nd/4.0/>).

analyses of epigenomic data from postmortem brain tissues of AD patients, we uncovered a significant alteration of CTCF binding on a genome-wide scale. Moreover, we found that the genes with reduced CTCF occupancy in AD were enriched in cell adhesion and synaptic organization, and their transcriptional expression was also significantly diminished in AD.

How could the diminished CTCF binding be associated with the reduced transcription of synaptic genes in AD? CTCF occupancy and CTCF-mediated chromatin loops can promote transcription initiation by recruiting RNA polymerase II (Chernukhin et al., 2007), preventing DNA methylation (Engel et al., 2006), marking boundaries of histone methylation domains (Barski et al., 2007), or regaining histone acetylation in postmitotic cells (Kang et al., 2020). From bioinformatic analyses of the ChIP-seq data of histone H3 lysine 27 acetylation (H3K27ac, an active enhancer mark linked to transcriptional activation), we found that genes with reduced H3K27ac in AD overlapped significantly with those with the diminished CTCF binding, and the common genes were enriched in synaptic organization. These data suggest that CTCF-mediated higher-order chromatin structure is altered in AD, which may contribute to the diminished histone acetylation and transcriptional activation of synaptic genes.

2. Material and methods

2.1. ChIP-seq data samples

CTCF and H3K27ac ChIP-seq data were acquired from ENCODE consortium's Rush Alzheimer's Disease study (ENCODE Project Consortium, 2012; Luo et al., 2020). Single-end ChIP-seq performed by the Bernstein Lab on human postmortem brain tissue (middle frontal area 46) with AD and control subjects (no Cognitive Impairment) was used for this study. We analyzed female AD ($n = 9$) and female control ($n = 9$) samples at the time of data availability. Both CTCF ChIP-seq and H3K27ac ChIP-seq data were derived from the same human samples. All sample information (ENCODE accession numbers, age, sex etc.) is available in Supplementary Table 8.

2.2. ChIP-seq differential peak analysis

Differential analysis was performed using DiffBind R package (v 3.2.5) (Ross-Innes et al., 2012). EdgeR methodology was used for comparing ChIPseq data that were normalized with 'trimmed mean of M values' (TMM) (Chen et al., 2016; McCarthy et al., 2012; Robinson et al., 2010). The cutoff threshold for significantly different peaks across groups was set at p -value ≤ 0.05 (two-sided Wilcoxon 'Mann-Whitney' test). ChIPseeker R package (Wang et al., 2022; Yu et al., 2015) annotated the identified ChIP-seq peaks with associated gene names derived from relative location on the human genome (hg38, promoter defined as ± 3 kb of transcription start site). Comparison heatmap of CTCF peak profiles of AD and Control groups and distribution of differential CTCF peaks were also generated using ChIPseeker. BigWig files of ChIP-seq data were generated with DeepTools (Ramírez et al., 2014) Python package and BedTools (Quinlan and Hall, 2010) UNIX suite. ChIP-seq landscapes were generated using BigWig files and Integrative Genomics Viewer (IGV) Web App [https://igv.org] (Robinson et al., 2011). H3K4me3 peaks were used as markers for gene promoter locations (Sharifi-Zarchi et al., 2017) and H3K27ac peaks were used to mark gene enhancer locations (Creyghton et al., 2010). The 3D Genome Browser and the available CTCF Hi-C contact map (Wang et al., 2018) were used to locate topologically associated domains (TADs).

2.3. Gene ontology (GO) analyses, protein-protein interactions (PPI) network and hub genes

Metascape [https://metascape.org] (Zhou et al., 2019) was used to identify enriched categories of the genes with differential CTCF peaks in

AD using default threshold parameters (overlap ≥ 3 , p -value ≤ 0.01 , enrichment ≥ 1.5). Metascape's Gene Prioritization by Evidence Counting (GPEC)(beta) machine learning algorithm was used to rank the enriched pathways. SynGO [https://www.syngoportal.org/] (Koopmans et al., 2019) analysis was used to identify the enrichment (p -value ≤ 0.01) of synaptic genes from top GO pathways. String database [https://string.db] (Szklarczyk et al., 2021) was used to create PPI network for genes in top enriched categories. CytoHubba (Chin et al., 2014) app in Cytoscape (version 3.9.0) (Shannon et al., 2003) was used to detect top ranking hub genes using the Maximal Clique Centrality algorithm.

2.4. Overlapping differential ChIP and gene expression

Microarray data from the dorsolateral PFC of 129 AD patients and 101 non-demented healthy controls (Harvard Brain Tissue Resource Center) (Zhang et al., 2013) were used for transcriptomic analysis. We used box plots generated by the 'AD Consensus Transcriptomics' ShinyApp (developed at Swarup lab by Sam Morabito) to compare microarray gene expression levels in control and AD samples (Morabito et al., 2020). InteractiveVenn [http://www.interactivennet/] (Heberle et al., 2015) was used to detect overlapping genes among gene sets acquired from differential ChIP-seq analysis and differential gene expression analysis. Heatmap of raw gene expression from the microarray data was generated using Phantassus [https://ctlab.itmo.ru/phantassus].

2.5. Chromatin immunoprecipitation-PCR (ChIP-PCR)

Postmortem human frontal cortex (Brodmann's area 10) from patients with AD (both males and females, Braak Stage V or VI) and age-matched control subjects were provided by the National Institutes of Health (NIH) NeuroBioBank. Upon arrival, tissue was stored in a -80°C freezer until use.

Human tissues were homogenized in 250 μl ice-cold douncing buffer (10 mM Tris-HCl, 4 mM MgCl₂, 1 mM CaCl₂, pH 7.5). Chromatin shearing used two approaches. In some experiments, the homogenized sample was incubated with 12.5 μl micrococcal nuclease (final conc. 5 U/ml, Sigma, N5386) for 7 min and terminated by adding EDTA (final conc. 10 mM). In other experiments, the homogenized sample was sonicated with Sonic Dismembrator Model 500 (Fisher Scientific) on ice (30% strength, 30-s each time, 5 times). Both methods gave similar results, so data were pooled together. After chromatin shearing, hypotonic lysis buffer (1 ml) was added and incubated on ice for 1 h. The supernatant was transferred to a new tube after centrifugation. After adding 10 \times incubation buffer (50 mM EDTA, 200 mM Tris-HCl, 500 mM NaCl), 10% of the supernatant was saved to serve as input control. To reduce nonspecific background, the supernatant was pre-cleared with 100 μl of salmon sperm DNA/protein A agarose-50% slurry (Millipore, 16-157) for 2 h at 4°C with agitation. The pre-cleared supernatant was incubated with antibodies against CTCF (3 μg per reaction; 07-729, Millipore/Sigma) overnight at 4°C under constant rotation, followed by incubation with 60 μl of Salmon Sperm DNA/Protein A agarose-50% Slurry for 2 h at 4°C . After washing for five times, bound complex was eluted twice from the beads by incubating with the elution buffer (100 μl) at room temperature. Proteins and RNA were removed by using proteinase K (Invitrogen) and RNase (Roche). Immunoprecipitated DNA and input DNA were purified by QIAquick PCR purification Kit (Qiagen). Quantification of ChIP signals was calculated as percent input. Purified DNA was subjected to qPCR reactions with primers against human *GRIN2A* enhancer (Forward, 5' CCACAGGTCCTACTCTTCCC 3'; Reverse, 5' GTGGTCATGGTTTCGCTGTC 3'), *GRIN2A* promoter (Forward, 5' GAGCCCTGATCTCCCTCTG 3'; Reverse, 5' CTAACCCGGTGGCTGCT 3'), *SHANK2* enhancer (Forward, 5' CTCCAGGGCTTTGTTTGTG 3'; Reverse, 5' TGCCCACTTTGCTAGAGTCA 3'), and *SHANK2* promoter (Forward, 5' CCTGGATGGGAGCTCTGC 3'; Reverse, 5' GTCTGCCCTTCTCTGGAA 3').

2.6. Statistical analyses

ChIP-seq Differential Analysis: statistically significant peaks in Diff-bind (measured by difference in read densities) were identified by EdgeR on a negative binomial distribution model to estimate variance. All peaks annotated were ranked by *p*-values that were computed using a two-sided Wilcoxon ‘Mann-Whitney’ test. CTCF peaks at individual genes across sample groups were compared using unpaired *t*-test with Welch’s correction.

Gene Ontology Pathway Enrichment Analysis: Metascape’s gene set

enrichment analysis uses the following equation to calculate the enriched pathways’ *p*-values derived from hypergeometric distribution. This *p* value is further corrected by Benjamini Hochberg correction to get False Discovery Rate (FDR).

$$p = \sum_{i=n}^{\min(M,K)} \binom{i}{n} \binom{N-k}{M-i}$$

Where N is total genes in human genome, M is total input genes, k is genes in selected pathway for analysis, and n is the genes common in k

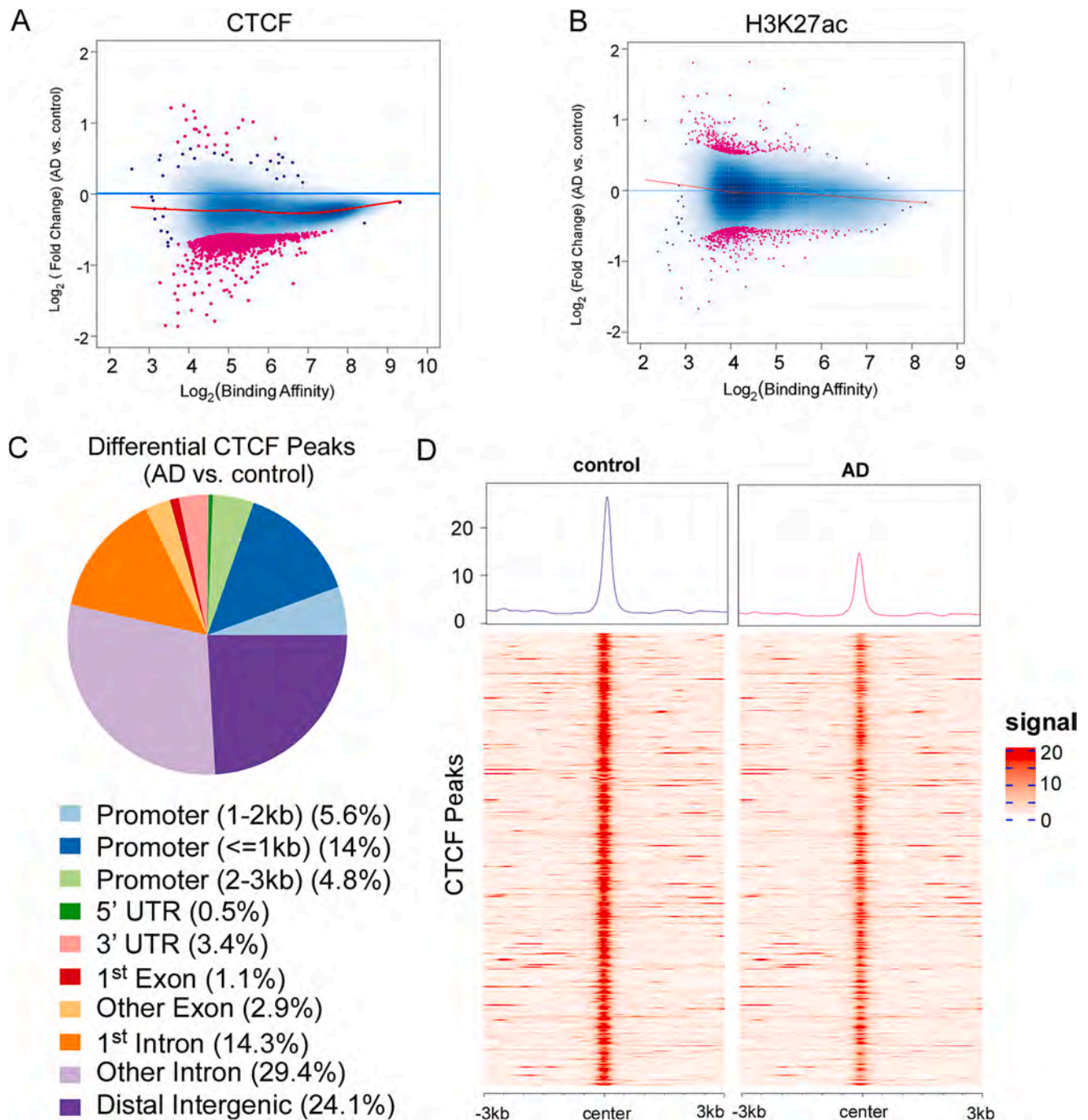


Fig. 1. Genome-wide CTCF binding is significantly diminished in frontal cortex of AD patients.

A, B, MA plot depicting fold changes over binding affinities for CTCF (A) or H3K27ac (B) in AD patients (n=9), compared to control samples (n=9). Pink dots indicate significantly differentially bound sites (*p* ≤ 0.05, two-sided Wilcoxon ‘Mann-Whitney’ test). C, Pie chart illustrating the locations of differentially bound CTCF sites in AD patients on the genome. D, CTCF ChIP-seq profile plots and heatmaps illustrating the significantly reduced CTCF binding sites (± 3Kb from peak centers) in AD patients, compared to control samples.

and M.

SynGO enrichment analysis was based on a combination of “Generalized Gene-Set Analysis of GWAS Datagene-set analysis (MAGMA)” (De Leeuw et al., 2015), “Stratified LD-Score Regression (S-LDSC)” (Finucane et al., 2015; Gazal et al., 2017) using brain expressed GWAS datasets (Koopmans et al., 2019).

Protein-Protein Interaction Network Analysis: STRING PPI analysis was used with medium confidence set as the cut-off for selected gene sets. Genes with no edges were removed. Modules were defined using gene enrichment analysis. To determine hub genes, we used CytoHubba’s MCC setting, which is based on how essential proteins are clustered. MCC of a node $v = \sum_{C \in S(v)} (|C| - 1)!$, where $S(v)$ = collection of maximal cliques containing v , and $(|C| - 1)!$ contains all positive integers less than $|C|$.

Microarray Differential Expression Analysis: Differential expression for microarray data was tested for statistical significance by limma classic t-statistic, and arranged by fold change, p-value and adjusted p-value (Benjamini-Horchberg).

Overlapping of Gene Lists: Hypergeometric test was used to calculate the p-value for under- or over-enrichment based on the cumulative distribution function (CDF). Expected number of successes = $(s^*M)/N$, s : sample size, M : number of successes in the population, N : population size. If k (actual number of successes) $> (s^*M)/N$, then k is considered over-enriched, otherwise under-enriched.

3. Results

3.1. AD patients have reduced CTCF binding affinity genome-wide in postmortem brains

We performed epigenomic analysis of CTCF ChIP-seq data of postmortem brain tissues (BA46 of prefrontal cortex) in control and AD patients ($n = 9$ pairs, all females) acquired from the ongoing ENCODE project by Rush University Alzheimer’s Disease Center (ENCODE Project Consortium, 2012). Using DiffBind R Bioconductor package, we found that 1742 out of 53,377 CTCF-binding peaks were significantly altered in AD samples (Supplementary Table 1), with 1719 reduced CTCF peaks and 23 increased CTCF peaks. While the majority of differential CTCF peaks showed the loss in AD samples, compared to controls (Fig. 1A), H3K27ac peaks showed both gain and loss in AD (Fig. 1B), suggesting that the marked reduction of CTCF occupancy in AD is not due to tissue qualities. The significant reduction of CTCF binding in AD was found at gene bodies, gene promoters and intergenic regions, and 24.4% was at the promoter (3 kb around TSS) (Fig. 1C). This reduction of CTCF binding on target genes in AD (Fig. 1D) could lead to changes in CTCF-mediated chromatin looping and genome architecture, resulting in altered gene expression.

3.2. Genes with reduced CTCF binding in AD are enriched in cell junction organization

Gene Ontology (GO) enrichment analyses of the 1241 genes with significantly reduced CTCF binding in AD indicated that the most prominently enriched biological processes are involved in the regulation of neuron projection, actin filaments, receptor signaling, cell adhesion and synaptic transmission (Fig. 2A, Supplementary Table 2), and the most enriched cellular components are postsynapse, axon, presynapse, actin cytoskeleton, and cell-cell junction (Fig. 2B).

Protein-Protein Interaction (PPI) network analyses indicated that genes with significantly reduced CTCF binding in AD are highly clustered in cell junction organization and actin cytoskeleton (Fig. 2C). Hub gene analysis was performed to identify key genes that represent the central molecular constituents most strongly connected in the gene network, which are presumably most responsible for the network’s global function. Using CytoHubba, which ranks proteins based on node features in the network, we found that hub genes with the highest

rankings were associated with synaptic organization, including *SHANK1/2*, *HOMER1* and *DLG2* (encoding scaffolding/anchoring proteins at glutamatergic synapses), *NRXN1* (encoding the pre- and post-synaptic membrane cell-adhesion molecule Neurexin 1), *ERBB4* (encoding receptor tyrosine kinase erbB-4 activated by Neuregulins), *GRIN2A* (encoding NMDAR subunit NR2A), and *GRM3* (encoding metabotropic glutamate receptor 3). Other notable synaptic genes with the reduction of CTCF binding include *CNTNAP2* (encoding a Contactin-associated protein in the Neurexin family), *NRXN3* (encoding Neurexin 3), *ERBB3* (encoding erbB-3), *STXBP6* (encoding Syntaxin Binding Protein 6), and *KALRN* (encoding Kalirin RhoGEF kinase that is important for spine formation) (Xie et al., 2007). One cluster of genes with reduced CTCF binding in AD, which is enriched in “cell junction organization & adhesion” category, was the protocadherin (*PCDHB9*, *PCDHB13*, *PCDHB14*) and cadherin (*CDH8*, *CDH13*, *CDH19*, *CDH24*) family members.

Among the genes with reduced CTCF binding in AD, which are enriched in the category of “cellular response to stress”, many are involved in chromosome organization and DNA repair, like the hub genes *POLE* and *POLE4* (encoding a DNA polymerase), *RFC2* (encoding a replication factor required by DNA polymerases for DNA elongation) and *ERCC* (encoding a DNA excision repair protein). In addition, many histone modifiers and chromatin remodelers were also found in this group, including *HDAC9*, *HAT1*, *KAT6B*, *KMT2A/C*, *KDM4B*, *SUV420H2*, *SETD7*, *DOT1L*, *PHF8*, *SMARCB1*, and *ARID1A*.

With cell junction organization being the most significantly enriched GO category for genes with reduced CTCF binding in AD, we utilized SynGo, a synaptic gene ontology database, to further explore dysregulated synaptic pathways in Alzheimer’s disease. Among the genes with reduced CTCF binding, 196 were classified as synaptic genes (Supplementary Table 3). Synaptic enrichment analyses identified synaptic organization, transport and signaling as the most enriched biological processes, while presynapse and postsynapse as the most enriched and abundant subcellular components, for synaptic genes with reduced CTCF binding in AD (Fig. 2D).

3.3. Reduced CTCF binding is linked to altered gene expression in AD

To find out whether the reduction of CTCF binding on target genes in AD is linked to their transcriptional alteration, we compared ChIP-seq data with transcriptomic analysis of microarray data from the dorsolateral PFC of 129 AD patients and 101 non-demented healthy controls (Harvard Brain Tissue Resource Center) (Zhang et al., 2013). With a cutoff of adjusted $p < 0.001$ and fold change (FC) of 10%, we identified 1516 downregulated genes in AD patients, which are enriched in synaptic signaling, synapse organization, ion transport, neurotransmitter secretion, and glutamatergic synaptic transmission (Williams et al., 2021). Among genes with reduced CTCF binding (1241) and genes with downregulated expression (1516) in AD, 101 overlapped genes were identified in the two groups (Fig. 3A, Supplementary Table 4). GO analyses of these common genes indicated that they were enriched in Biological Processes like axon guidance, regulation of neural transmission, trans-synaptic signaling, postsynaptic organization and synaptic adhesion, and Cellular Components like pre- and post-synaptic membrane and transmembrane transporter complex (Fig. 3B). PPI of these common genes in top GO pathways pointed to key synaptic genes, such as *GRIN2A*, *SHANK2*, *NRXN1*, *SNAP91*, and *CNTNAP2* (Fig. 3C).

On the other hand, we identified 1134 upregulated genes in AD patients, which are enriched in immune response activation and cell death (Williams et al., 2021). Only 64 overlapped genes were identified between genes with reduced CTCF binding (1241) and genes with upregulated expression (1134) in AD (Fig. 3D). These common genes were enriched in T-cell activation, MAPK cascade and actin cytoskeleton polymerization (Fig. 3E).

Next, we examined the expression of selected genes with reduced CTCF binding in the 3 major GO pathways: synaptic organization, cell

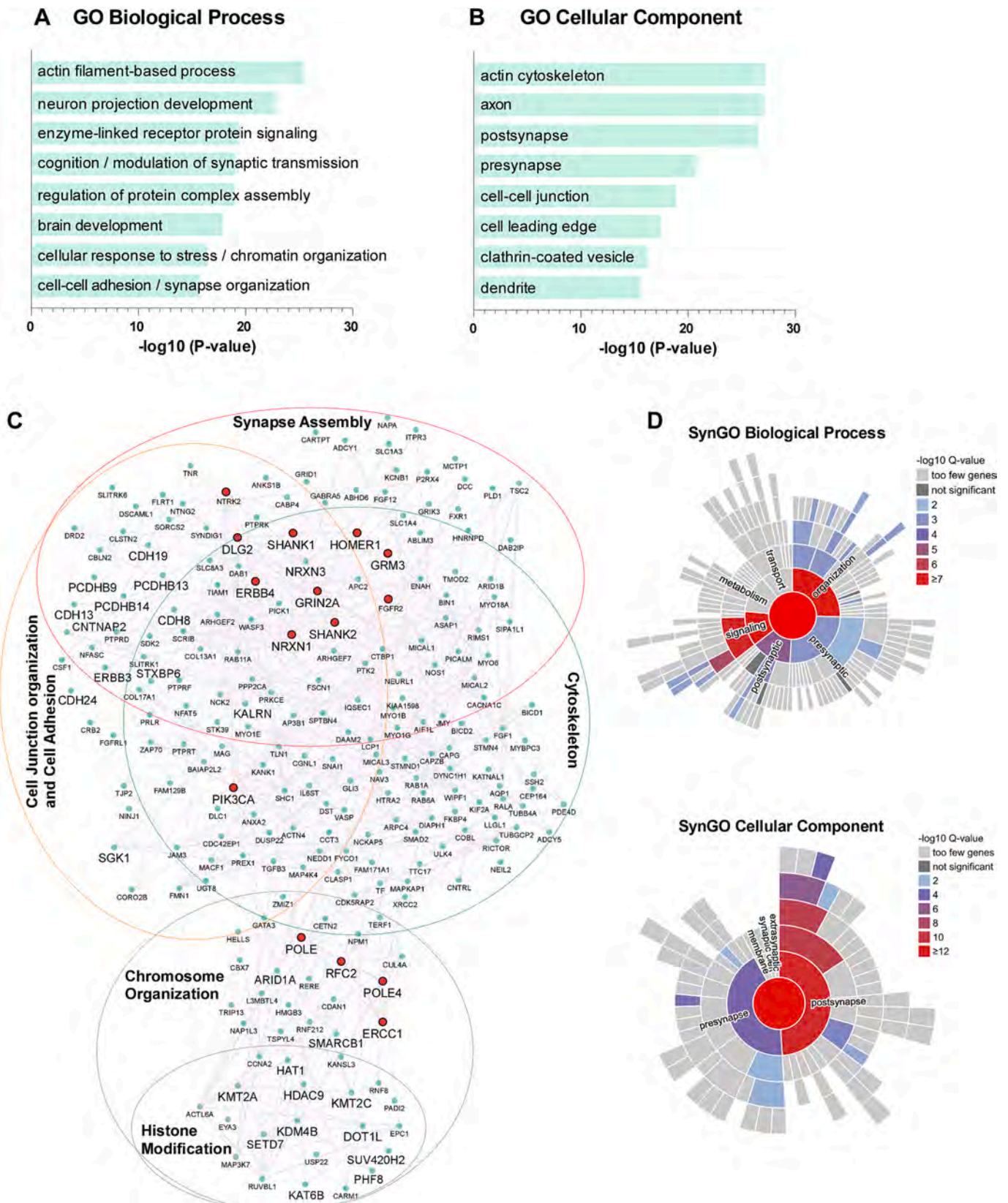


Fig. 2. Genes with the significantly reduced CTCF binding in AD are enriched in synaptic organization, cell adhesion and actin cytoskeleton. **A, B,** Gene Ontology (GO) analysis with Metascape depicting the most enriched categories in Biological Processes (A) or Cellular Component (B) of all the genes with significantly reduced CTCF binding in AD patients. **C,** Protein-Protein Interaction (PPI) networks of genes with significantly reduced CTCF binding in AD among the top 8 GO categories. HUB genes are highlighted with red. **D,** Sunburst plot from SynGO analysis illustrating the most enriched categories in Biological Processes (top) or Cellular Component (bottom) of the synaptic genes with significantly reduced CTCF binding in AD among the top 8 GO categories. Higher red intensities are associated with more significant enrichments.

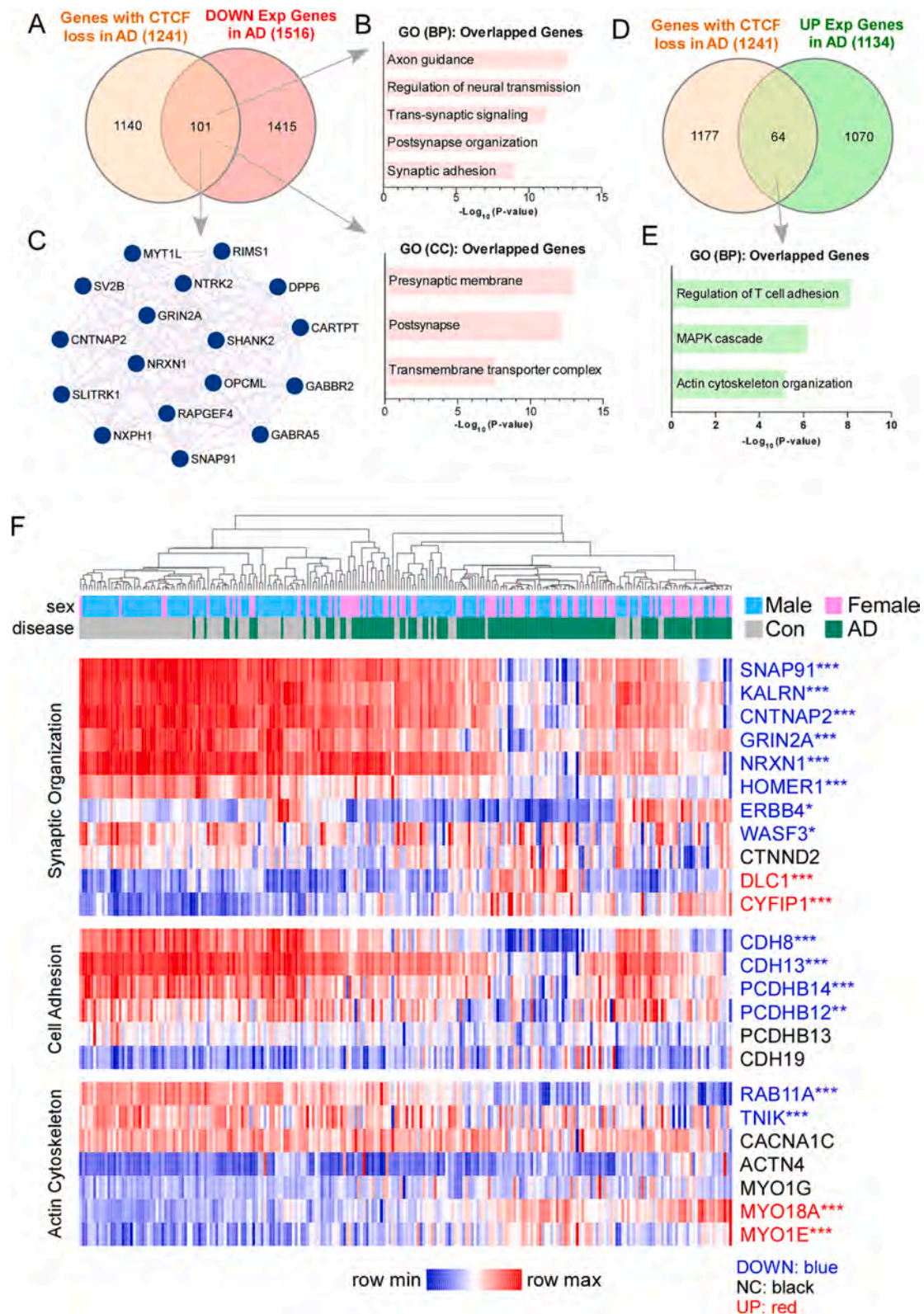


Fig. 3. Genes with reduced CTCF binding in AD show altered mRNA expression in AD.

A, D, Venn diagrams showing the overlap of genes with reduced CTCF binding in AD and genes with downregulated (**A**) or upregulated (**D**) expression in AD from Microarray data. **B, E,** Gene Ontology (GO) showing the enriched pathways of overlapped genes with reduced CTCF binding and down-regulated (**B**) or up-regulated (**E**) expression in AD. BP: Biological Processes; CC: Cellular Component. **C,** PPI networks of overlapped genes with reduced CTCF binding and down-regulated expression in AD. **F,** Heatmaps showing the expression of selected genes with reduced CTCF binding in AD in top GO pathways (synaptic organization, cell adhesion, and actin cytoskeleton) in control (n=101) vs. AD (n=129) samples. Red: Down-regulated genes; Black: non-changed genes; Green: Up-regulated genes.

adhesion, actin cytoskeleton. As shown in Fig. 3F, compared to controls ($n = 101$), most of the synaptic and adhesion genes exhibited a consistent reduction of the mRNA expression value in AD patients ($n = 129$), including *GRIN2A*, *NRXN1*, *HOMER1*, *SNAP91*, *KALRN*, *ERBB4*, *CNTNAP2*, *CDH8*, *CDH13*, *PCDH12*, *PCDH14*, while actin cytoskeleton genes exhibited 3 patterns (DOWN, No Change, UP). These data suggest that the diminished CTCF binding on synaptic and adhesion genes may contribute to their transcriptional reduction in AD.

3.4. Genes in cell adhesion and synaptic organization have reduced CTCF binding and expression in AD

To better understand the relationship between CTCF binding and gene expression, we further examined the ChIP-seq and transcriptomic data of a few key genes involved in cell adhesion or synaptic organization. As shown in representative landscapes of CTCF occupancies at the clustered protocadherin gene locus from a control subject and an AD

patient (Fig. 4A), CTCF peaks at *PCDH α* , *PCDH β* and *PCDH γ* family members were markedly reduced in the AD sample. Significant differences of CTCF occupancy at *PCDH α* , *PCDH β* and *PCDH γ* were observed between control and AD patients ($n = 9/\text{group}$) (Fig. 4B). Similarly, CTCF occupancies at *CDH8*, *CDH13* and *CDH19* were significantly reduced in AD patients, compared to controls (Fig. 4C and 4D). Microarray data (Fig. 4E) also revealed the significant reduction of protocadherin genes (*PCDH α 6*, *PCDH β 12*) and cadherin genes (*CDH8*, *CDH13*) in AD, while *CDH19* expression was not reduced in AD patients.

Hi-C probing of 3D genome architecture has identified ~10,000 CTCF-bound loops that typically occur at contact domain boundaries, which frequently link promoters and enhancers, influencing gene activation (Rao et al., 2014). Hi-C interaction matrices at a topologically associating domain (TAD) encompassing *GRIN2A* locus show the intense contacts demarcated by CTCF-bound loops within the gene body and with other neighboring genes (Fig. 5A). CTCF peaks at *GRIN2A* promoter (marked by H3K4me3), two enhancers (marked by H3K27ac), and a

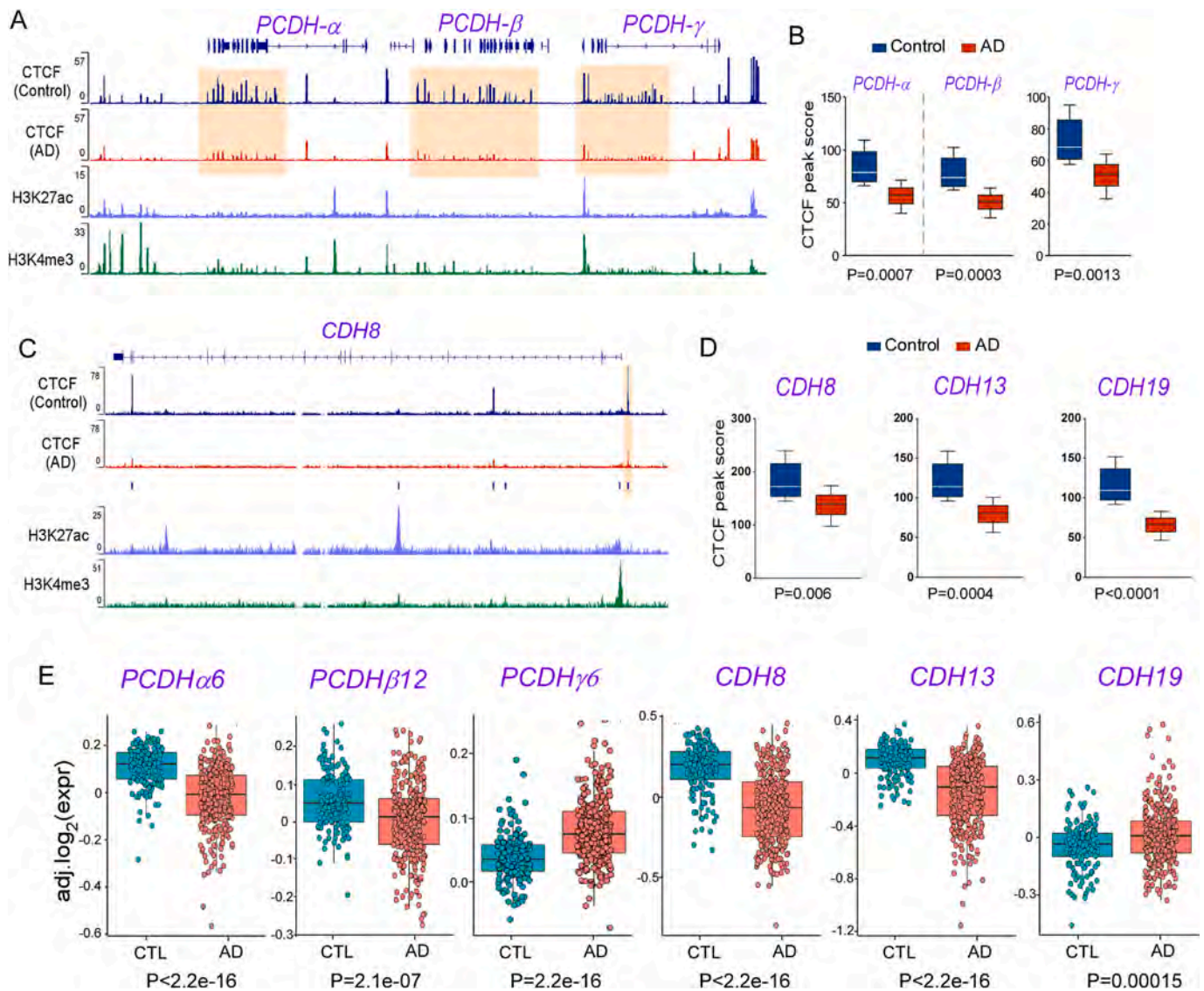


Fig. 4. Cell adhesion genes in protocadherin and cadherin families show the reduced CTCF binding and expression in AD.

A, C, Epigenome browser snapshots of ChIP-seq data showing the landscape of CTCF peaks at the clustered protocadherin gene locus encompassing *PCDH α* , *PCDH β* and *PCDH γ* family members (A) or at cadherin 8 (*CDH8*) gene locus (C) in PFC from a control and an AD patient. The landscape of H3K4me3 and H3K27ac binding sites are also shown to illustrate the promoter and enhancer regions. **B, D,** Box plots showing CTCF peak scores from differential peak calling analysis with DiffBind at *PCDH α* , *PCDH β* and *PCDH γ* (B) or cadherin genes including *CDH8*, *CDH13*, and *CDH19* (D) in control vs. AD samples ($n=9$ pairs, unpaired t-test with Welch's correction). **E,** Box plots showing mRNA expression levels of selected protocadherin and cadherin genes in control vs. AD samples from microarray data (control: $n=101$; AD: $n=129$, unpaired t test with Welch's correction).

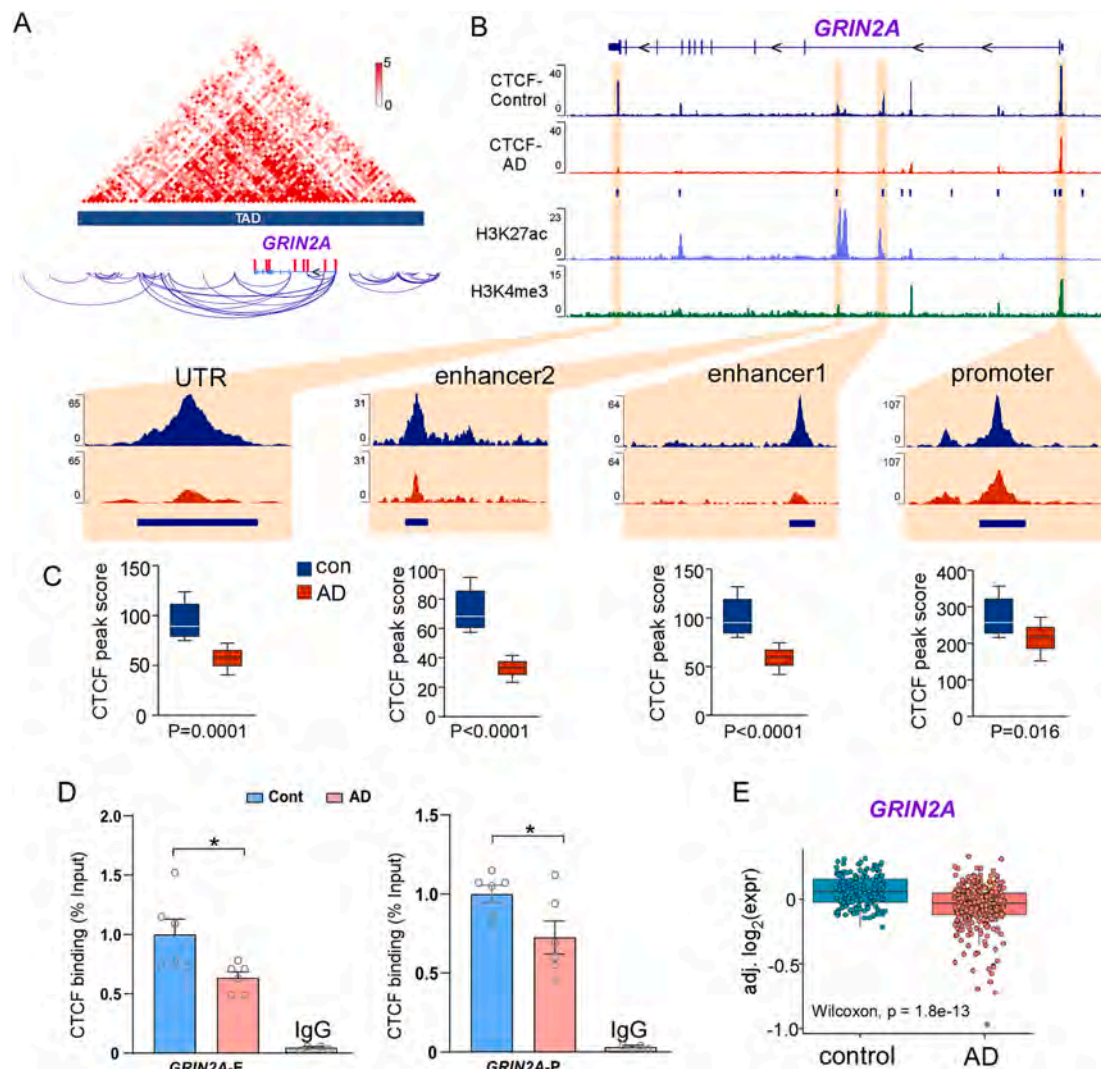


Fig. 5. Synaptic gene *GRIN2A* has the reduced CTCF binding and expression in AD.

A, Heatmaps of contact matrices from Hi-C data at a topologically associating domain (TAD) encompassing *GRIN2A* locus. CTCF binding sites on *GRIN2A* are labeled with red pins. Each curved line connects two noncontiguous DNA segments. **B**, Epigenome browser snapshots of ChIP-seq data showing the landscape of CTCF peaks at *GRIN2A* gene locus in a control and an AD patient. The landscape of H3K4me3 and H3K27ac are also shown to illustrate the promoter and enhancer regions. Zoomed in CTCF peaks at specific loci are shown below. **C**, Box plots showing CTCF peak scores for differential peak calling analysis with DiffBind at the promoter and enhancer regions of *GRIN2A* in control vs. AD samples ($n=9$ pairs, unpaired t-test with Welch's correction). All the p values are from unpaired t test with Welch's correction. **D**, Bar graphs showing ChIP-PCR quantification of CTCF occupancy at *GRIN2A* enhancer 1 (E) or promoter (P) in PFC from control vs. AD patients ($n=6$ /group, $p=0.024$ (E), $p=0.042$ (P), unpaired t-test with Welch's correction). IgG controls are also shown to demonstrate the specificity of the ChIP-PCR data on CTCF binding. **E**, Box plots showing mRNA expression levels of *GRIN2A* in control vs. AD samples from microarray data (control: $n=101$; AD: $n=129$, unpaired t test with Welch's correction).

UTR region were significantly reduced in AD samples (Fig. 5B and 5C). We then performed ChIP-PCR assays of postmortem PFC from AD patients to validate whether CTCF binding on *GRIN2A* was indeed decreased. As shown in Fig. 5D, the CTCF peak score was significantly lower at the enhancer and promoter regions of *GRIN2A* in AD patients, compared to control subjects, consistent with the CTCF ChIP-seq epigenomic data (ENCODE Project Consortium, 2012). Concomitant with the reduction of CTCF binding on *GRIN2A*, the expression level of *GRIN2A* (Fig. 5E) was significantly lower in AD samples ($n = 129$), compared to controls ($n = 101$).

Hi-C contact map also reveals the contacts at a TAD encompassing *SHANK2* locus, which are composed of two separate clustered CTCF-bound chromatin loops (Fig. 6A). A marked reduction of CTCF binding at the promoter and enhancer of *SHANK2* was found in AD patients (Fig. 6B and 6C). ChIP-PCR assays validated the significant decrease of CTCF peaks at *SHANK2* enhancer and promoter in AD patients (Fig. 6D).

Moreover, the expression level of *SHANK2* (Fig. 6E) was significantly lower in AD samples. Taken together, these data suggest that the significantly diminished CTCF binding on adhesion and synaptic genes in AD may be responsible for their transcriptional repression due to the attenuation of chromatin looping to bring together promoters and enhancers.

3.5. Genes with reduced CTCF binding and reduced histone acetylation in AD converge on synaptic pathways

Next, we further explored the potential molecular mechanism underlying the link of synaptic genes with reduced CTCF occupancy in AD to their diminished mRNA expression. CTCF is known to be able to control gene expression via diverse avenues, including the recruitment of transcriptional machinery and the regulation of DNA methylation or histone modifications (Chernukhin et al., 2007) (Barski et al., 2007;

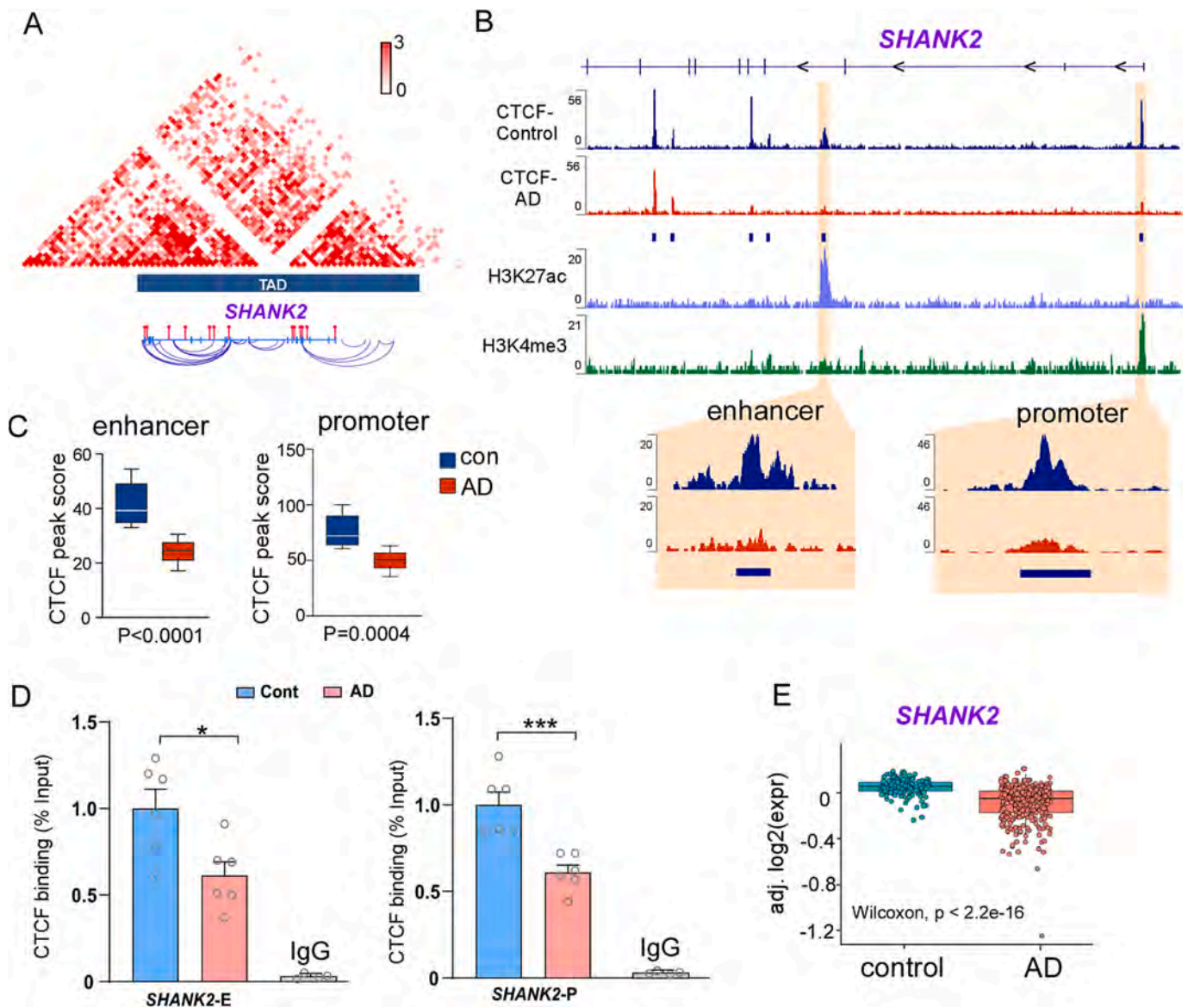


Fig. 6. Synaptic gene *SHANK2* has the reduced CTCF binding and expression in AD. **A**, Heatmaps of contact matrices from Hi-C data at a TAD encompassing *SHANK2* locus. CTCF binding sites on *SHANK2* are labeled with red pins. **B**, Epigenome browser snapshots of ChIP-seq data showing the landscape of CTCF peaks at *SHANK2* gene locus in a control and an AD patient. **C**, Box plots showing CTCF peak scores at the promoter and enhancer regions of *SHANK2* in control vs. AD samples ($n=9$ pairs, unpaired t-test with Welch's correction). **D**, Bar graphs showing ChIP-PCR quantification of CTCF occupancy at *SHANK2* enhancer (E) or promoter (P) in PFC from control vs. AD patients ($n=6$ /group, $p=0.017$ (E), $p=0.001$ (P), unpaired t-test with Welch's correction). IgG controls are also shown. **E**, Box plots showing mRNA expression levels of *SHANK2* in control vs. AD samples from microarray data (control: $n=101$; AD: $n=129$, unpaired t test with Welch's correction).

Engel et al., 2006; Kang et al., 2020). Thus, we examined ChIP-seq data of H3K27ac (an active enhancer mark) from postmortem PFC of control and AD patients ($n = 9$ pairs) acquired from the ENCODE project (ENCODE Project Consortium, 2012), and compared them with CTCF ChIP-seq data. We found that 788 H3K27ac peaks were significantly reduced and 542 H3K27ac peaks were significantly increased in AD samples (fold change: $\geq 10\%$; $P \leq 0.05$), with 502 genes showing H3K27ac losses and 448 genes showing H3K27ac gains (Supplementary Table 5).

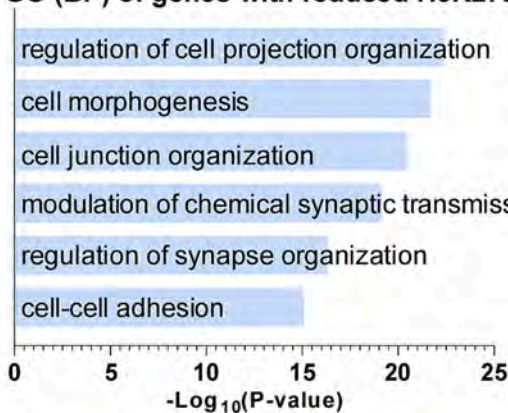
GO enrichment analyses indicated that genes with significantly reduced H3K27ac in AD were enriched in cell junction organization and synaptic transmission (Fig. 7A). Among genes with reduced CTCF binding (1241) and genes with reduced H3K27ac (502) in AD, a significant overlap (99 overlapped genes) was identified (Fig. 7B, Supplementary Table 6), which represents 2.7-fold over-enrichment in

overlapping genes. Moreover, the common genes are enriched in the regulation of synapse organization and membrane potential (Fig. 7C, Supplementary Table 7). The top 30 overlapping hub genes were key players in synaptic organization and function, including *NRXN1*, *HOMER1*, *CTNND2*, and *SV2B* (Fig. 7D). These data suggest that CTCF binding may affect the expression of synaptic genes via a mechanism involving the facilitation of histone acetylation, and the reduction of CTCF binding in AD leads to histone deacetylation and transcriptional reduction.

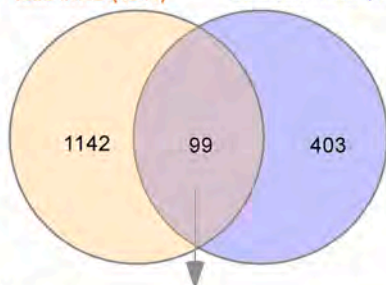
4. Discussion

From proteomic studies of two longitudinal cohorts, it has been found that the increased abundance of synaptic genes is required for cognitive stability (Wingo et al., 2019). It suggests that the diminished

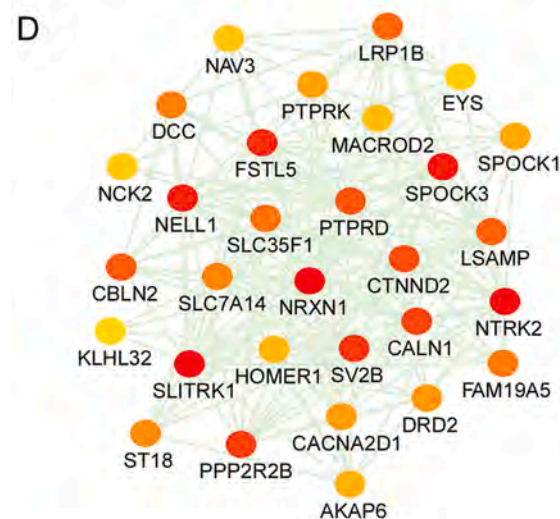
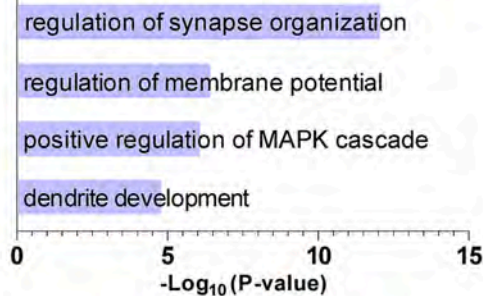
A GO (BP) of genes with reduced H3K27ac in AD



B Genes with CTCF loss in AD (1241) vs Genes with reduced H3K27ac in AD (502)



C GO pathways of the overlapped genes with reduced CTCF binding and H3K27ac occupancy in AD



(caption on next column)

Fig. 7. Genes with reduced H3K27ac overlap with genes with reduced CTCF binding in AD, and the common genes are enriched in synaptic organization. **A**, Gene Ontology (GO) showing the enriched pathways in Biological Processes (BP) of genes with decreased H3K27ac occupancy in AD patients (n=9), compared to control samples (n=9). **B**, Venn diagrams showing the overlap of genes with reduced CTCF binding and genes with decreased H3K27ac occupancy in AD. $p = 3.18e-20$, hypergeometric test. **C**, GO pathways of the overlapped genes with reduced CTCF binding and H3K27ac occupancy in AD. **D**, PPI of top 30 overlapped hub genes with reduced CTCF binding and H3K27ac occupancy in AD. Higher red intensities are associated with higher rankings.

expression of synaptic genes important for neuronal plasticity is responsible for cognitive decline in AD (Williams et al., 2021). For the discovery of therapeutic strategies to counteract AD progression, it is important to uncover how the transcription of synaptic genes is impaired in AD.

In chromosome of eukaryotes, DNA is wrapped around histones to form the nucleosomal fiber, which is further folded and looped into sophisticated higher-order three-dimensional structures. This 3D chromatin organization is controlled by CTCF, the master genome architecture protein that has crucial roles in the regulation of chromatin structure and gene transcription, including context-dependent promoter activation/repression, enhancer blocking and/or barrier insulation, and long-range chromatin interactions (Bell et al., 1999; de Wit et al., 2015; Dixon et al., 2012; Hou et al., 2008; Merckenschlager and Odom, 2013; Phillips and Corces, 2009). It has been found that CTCF binding at the proximal promoter facilitates distal enhancer-dependent gene activation (Kubo et al., 2021), thus, the alteration of CTCF occupancy at gene promoters could directly affect transcriptional outcomes.

Our epigenetic analyses of CTCF ChIP-seq data have identified a genome-wide reduction of CTCF binding in postmortem PFC of AD patients (n = 9), compared to control subjects (n = 9). Interestingly, genes with reduced CTCF binding in AD are enriched in synapse organization and cell junction assembly, including protocadherin (*PCDH*) and cadherin (*CDH*) family members, synaptic scaffolding/anchoring molecules or receptors such as *SHANK2*, *GRIN2A*, *HOMER1*, and *NRXN1*. These results have suggested a potential alteration of CTCF function in AD.

By comparing transcriptomic data from AD patients (Zhang et al., 2013), we have discovered that many of the adhesion and synaptic genes with reduced CTCF binding in AD are significantly diminished in their mRNA expression. For example, CTCF occupancies at the clustered protocadherin (*PCDH*) gene locus containing *PCDHα*, *PCDHβ* and *PCDHγ* were markedly reduced in AD patients, which was correlated with their transcriptional loss in AD. The expression of distinct repertoires of protocadherin protein isoforms serves as cell-surface molecular barcodes for neural circuit assembly (Canzio and Maniatis, 2019; Mounoufari et al., 2018). CTCF is found to be heavily involved in promoter-enhancer interactions to regulate the expression of *PCDH* in neurons (Hirayama, 2012). Binding of the CTCF/cohesin complex and DNA looping to a distant enhancer is one of the mechanisms underlying stochastic expression of individual *Pcdhα* isoforms (Canzio and Maniatis, 2019), which generates enormous molecular diversity at the cell surface. The reduction of CTCF occupancy at *PCDH* gene locus in AD could lead to the disruption of molecular recognition codes and synaptic interactions among neurons.

Additional target genes with the significantly diminished CTCF binding and transcription in AD include *GRIN2A* and *SHANK2*, both of which are key components of the NMDAR complex involved in synaptic plasticity directly linked to cognition and memory. CTCF occupancy at the promoter and enhancer of *GRIN2A* and *SHANK2* was significantly abrogated in AD, suggesting that these genes have lost CTCF-mediated chromatin looping to bring together promoters and enhancers, which could result in their diminished transcriptional activation in AD.

To better understand how the reduction of CTCF binding is linked to transcriptional changes in AD, we compared CTCF and H3K27ac ChIP-seq data in AD brains, as the increase of H3K27ac may play a role in

the establishment of topologically associating domains (TADs) demarcated by CTCF during postmitotic transcriptional reactivation (Kang et al., 2020). Emerging evidence also implicates the alterations of histone acetylation and methylation in AD pathophysiology (Cao et al., 2020; Gräff et al., 2012; Nativio et al., 2020; Wang et al., 2021; Zheng et al., 2019). We have found altered H3K27ac peaks in AD patients, with both gains and losses (40.8% gains in peaks, 59.2% losses in peaks). It is slightly different from another epigenomic profiling, which found more gains than losses of H3K27ac peaks (57.6% gains, 42.4% losses) in AD (Nativio et al., 2020). The differences in human samples and selection criteria may underlie the discrepancy. We have identified a significant overlap of genes with the reduced CTCF binding and the reduced H3K27ac in AD, with the common genes enriched in synaptic organization. It is plausible that the reduced CTCF occupancy in AD changes the higher-order chromatin structure at specific genomic loci, causing the altered recruitment or binding of histone acetyltransferases or deacetylases, which results in the diminished transcriptional activation of target genes.

H3K4me3, an epigenetic mark associated with actively transcribing genes, plays a key role in regulating the expression of synaptic genes (Dincer et al., 2015). Thus, another epigenomic mechanism that may affect the transcription of synaptic genes in AD is the alteration of neuronal H3K4me3 epigenome. Genome-wide mapping has identified extensive H3K4me3 reorganization on neuronal genes at the early developmental stage in PFC (Cheung et al., 2010). Aberrant localization of H3K4me3 was found early in the course of AD (Mastroeni et al., 2015). Our discoveries on H3K4me3 alterations on genes regulating neuronal and synaptic functions in AD mouse models (Cao et al., 2020; Williams et al., 2023) also support the involvement of epigenetic abnormalities in neurodegenerative disorders.

Given the heterogeneity of human samples, the relatively small sample size of CTCF ChIP-seq data is a main limitation of this study, which only allows us to use a moderately stringent criterion in the differential CTCF peak analysis, as what has been used in a prior study for differential analyses of H3K27ac and H3K9ac peaks in control vs. AD patients (Nativio et al., 2020). With more epigenomic sequencing of a larger sample size, we will have more statistical power to determine what changes are more robust and what changes are not generally applicable.

In summary, this study has provided the first report revealing the binding changes of CTCF on genes involved in synaptic organization in AD human samples. Given the central role of CTCF in controlling genome architecture, it is possible that 3D chromatin organization at CTCF-binding genomic regions is altered in AD, which awaits to be tested in future studies using chromosome conformation capture techniques. Our finding has also provided a potential mechanism underlying the altered expression of synaptic genes in AD, which may directly contribute to synaptic dysfunction in this neurodegenerative disorder.

Supplementary data to this article can be found online at <https://doi.org/10.1016/j.nbd.2023.106192>.

Fundings

This work was supported by NIH grants AG064656 and AG079797 to Z.Y.

Disclosures

The authors report no competing financial or other interests.

Contributors

P.J.P.: Conceptualization, epigenomic and transcriptomic Data curation and Formal analysis. Y.R.: ChIP-PCR data curation and Formal analysis. Z.Y.: Conceptualization, Project administration, Supervision, Writing the paper and Funding acquisition.

Data availability

The ChIP-seq data analyzed here have been deposited in the ENCODE public repository under accession codes listed in Supplementary Table 8, and can be accessed directly. The differential peak scores for CTCF and H3K27ac ChIP-seq data are deposited as matrix dataframes into a public repository.

Acknowledgements

We are grateful to Dr. Jamal B. Williams for the introductory training of bioinformatic analysis packages. The work was supported by Center for Computational Research (CCR). We would also like to thank Drs. Ram Samudrala, Zackary Falls and their lab members for guiding us on how to use CCR resources and for statistical insights.

References

- Barski, A., et al., 2007. High-resolution profiling of histone methylations in the human genome. *Cell*. 129, 823–837.
- Bell, A.C., et al., 1999. The protein CTCF is required for the enhancer blocking activity of vertebrate insulators. *Cell*. 98, 387–396.
- Borrelli, E., et al., 2008. Decoding the epigenetic language of neuronal plasticity. *Neuron*. 60, 961–974.
- Canzio, D., Maniatis, T., 2019. The generation of a protocadherin cell-surface recognition code for neural circuit assembly. *Curr. Opin. Neurobiol.* 59, 213–220.
- Cao, Q., et al., 2020. Targeting histone K4 trimethylation for treatment of cognitive and synaptic deficits in mouse models of Alzheimer's disease. *Sci. Adv.* 6.
- Chen, Y., et al., 2016. From reads to genes to pathways: differential expression analysis of RNA-Seq experiments using Rsubread and the edgeR quasi-likelihood pipeline. *F1000Research*. 5, 1438.
- Chernukhin, I., et al., 2007. CTCF interacts with and recruits the largest subunit of RNA polymerase II to CTCF target sites genome-wide. *Mol. Cell Biol.* 27, 1631–1648.
- Cheung, I., et al., 2010. Developmental regulation and individual differences of neuronal H3K4me3 epigenomes in the prefrontal cortex. *Proc. Natl. Acad. Sci. U. S. A.* 107, 8824–8829.
- Chin, C.-H., et al., 2014. cytoHubba: identifying hub objects and sub-networks from complex interactome. *BMC Syst. Biol.* 8, S11.
- Creyghton, M.P., et al., 2010. Histone H3K27ac separates active from poised enhancers and predicts developmental state. *Proc. Natl. Acad. Sci.* 107, 21931–21936.
- De Leeuw, C.A., et al., 2015. MAGMA: generalized gene-set analysis of GWAS data. *PLoS Comput. Biol.* 11, e1004219.
- de Wit, E., et al., 2015. CTCF binding polarity determines chromatin looping. *Mol. Cell* 60, 676–684.
- Dehingia, B., et al., 2022. CTCF shapes chromatin structure and gene expression in health and disease. *EMBO Rep.* 23, e55146.
- Dincer, A., et al., 2015. Deciphering H3K4me3 broad domains associated with gene-regulatory networks and conserved epigenomic landscapes in the human brain. *Transl. Psychiatry* 5, e679.
- Dixon, J.R., et al., 2012. Topological domains in mammalian genomes identified by analysis of chromatin interactions. *Nature*. 485, 376–380.
- ENCODE Project Consortium, 2012. An integrated encyclopedia of DNA elements in the human genome. *Nature*. 489, 57–74.
- Engel, N., et al., 2006. CTCF binding sites promote transcription initiation and prevent DNA methylation on the maternal allele at the imprinted H19/Igf2 locus. *Hum. Mol. Genet.* 15, 2945–2954.
- Finucane, H.K., et al., 2015. Partitioning heritability by functional annotation using genome-wide association summary statistics. *Nat. Genet.* 47, 1228–1235.
- Fraser, P., Bickmore, W., 2007. Nuclear organization of the genome and the potential for gene regulation. *Nature*. 447, 413–417.
- Gazal, S., et al., 2017. Linkage disequilibrium-dependent architecture of human complex traits shows action of negative selection. *Nat. Genet.* 49, 1421–1427.
- Gräff, J., et al., 2012. An epigenetic blockade of cognitive functions in the neurodegenerating brain. *Nature*. 483, 222–226.
- Heberle, H., et al., 2015. InteractiVenn: a web-based tool for the analysis of sets through Venn diagrams. *BMC Bioinform.* 16.
- Hirayama, T., 2012. CTCF is required for neural development and stochastic expression of clustered Pcdh genes in neurons. *Cell Rep.* 2, 345–357.
- Hou, C., et al., 2008. CTCF-dependent enhancer-blocking by alternative chromatin loop formation. *Proc. Natl. Acad. Sci. U. S. A.* 105, 20398–20403.
- Kang, H., et al., 2020. Dynamic regulation of histone modifications and long-range chromosomal interactions during postmitotic transcriptional reactivation. *Genes Dev.* 34, 913–930.
- Konrad, E.D.H., et al., 2019. CTCF variants in 39 individuals with a variable neurodevelopmental disorder broaden the mutational and clinical spectrum. *Genet. Med.* 21, 2723–2733.
- Koopmans, F., et al., 2019. SynGO: an evidence-based, expert-curated Knowledge Base for the synapse. *Neuron*. 103, 217–234.e4.
- Kubo, N., et al., 2021. Promoter-proximal CTCF binding promotes distal enhancer-dependent gene activation. *Nat. Struct. Mol. Biol.* 28, 152–161.

- Lancôt, C., et al., 2007. Dynamic genome architecture in the nuclear space: regulation of gene expression in three dimensions. *Nat. Rev. Genet.* 8, 104–115.
- Lieberman-Aiden, E., et al., 2009. Comprehensive mapping of long-range interactions reveals folding principles of the human genome. *Science*. 326, 289–293.
- López-Otín, C., et al., 2023. Hallmarks of aging: an expanding universe. *Cell*. 186, 243–278.
- Luo, Y., et al., 2020. New developments on the encyclopedia of DNA elements (ENCODE) data portal. *Nucleic Acids Res.* 48, D882–D889.
- Mastroeni, D., et al., 2015. Aberrant intracellular localization of H3k4me3 demonstrates an early epigenetic phenomenon in Alzheimer's disease. *Neurobiol. Aging* 36, 3121–3129.
- Mathys, H., et al., 2019. Single-cell transcriptomic analysis of Alzheimer's disease. *Nature*. 570, 332–337.
- McCarthy, D.J., et al., 2012. Differential expression analysis of multifactor RNA-Seq experiments with respect to biological variation. *Nucleic Acids Res.* 40, 4288–4297.
- Merkenschlager, M., Duncan, 2013. CTCF and Cohesin: linking gene regulatory elements with their targets. *Cell*. 152, 1285–1297.
- Merkenschlager, M., Odom, D.T., 2013. CTCF and cohesin: linking gene regulatory elements with their targets. *Cell*. 152, 1285–1297.
- Morabito, S., et al., 2020. Integrative genomics approach identifies conserved transcriptomic networks in Alzheimer's disease. *Hum. Mol. Genet.* 29, 2899–2919.
- Mountoufaris, G., et al., 2018. Writing, Reading, and translating the clustered Protocadherin cell surface recognition code for neural circuit assembly. *Annu. Rev. Cell Dev. Biol.* 34, 471–493.
- Nativio, R., et al., 2020. An integrated multi-omics approach identifies epigenetic alterations associated with Alzheimer's disease. *Nat. Genet.* 52, 1024–1035.
- Nora, E.P., et al., 2017. Targeted degradation of CTCF decouples local insulation of chromosome domains from genomic compartmentalization. *Cell*. 169, 930–944.e22.
- Ohlsson, R., et al., 2001. CTCF is a uniquely versatile transcription regulator linked to epigenetics and disease. *Trends Genet.* 17, 520–527.
- Ohlsson, R., et al., 2010. Does CTCF mediate between nuclear organization and gene expression? *BioEssays*. 32, 37–50.
- Ong, C.-T., Corces, V.G., 2014. CTCF: an architectural protein bridging genome topology and function. *Nat. Rev. Genet.* 15, 234–246.
- Phillips, J.E., Corces, V.G., 2009. CTCF: master weaver of the genome. *Cell*. 137, 1194–1211.
- Quinlan, A.R., Hall, I.M., 2010. BEDTools: a flexible suite of utilities for comparing genomic features. *Bioinformatics*. 26, 841–842.
- Ramírez, F., et al., 2014. deepTools: a flexible platform for exploring deep-sequencing data. *Nucleic Acids Res.* 42, W187–W191.
- Rao, S.S., et al., 2014. A 3D map of the human genome at kilobase resolution reveals principles of chromatin looping. *Cell*. 159, 1665–1680.
- Robinson, M.D., et al., 2010. edgeR: a Bioconductor package for differential expression analysis of digital gene expression data. *Bioinformatics*. 26, 139–140.
- Robinson, J.T., et al., 2011. Integrative genomics viewer. *Nat. Biotechnol.* 29, 24–26.
- Ross-Innes, C.S., et al., 2012. Differential oestrogen receptor binding is associated with clinical outcome in breast cancer. *Nature*. 481, 389–393.
- Selkoe, D.J., 2002. Alzheimer's disease is a synaptic failure. *Science*. 298, 789–791.
- Shannon, P., et al., 2003. Cytoscape: a software environment for integrated models of biomolecular interaction networks. *Genome Res.* 13, 2498–2504.
- Sharifi-Zarchi, A., et al., 2017. DNA methylation regulates discrimination of enhancers from promoters through a H3K4me1-H3K4me3 seesaw mechanism. *BMC Genomics* 18.
- Szklarczyk, D., et al., 2021. The STRING database in 2021: customizable protein–protein networks, and functional characterization of user-uploaded gene/measurement sets. *Nucleic Acids Res.* 49, D605–D612.
- Tracy, T.E., Gan, L., 2018. Tau-mediated synaptic and neuronal dysfunction in neurodegenerative disease. *Curr. Opin. Neurobiol.* 51, 134–138.
- Vostrov, A.A., Quitschke, W.W., 1997. The zinc finger protein CTCF binds to the APBbeta domain of the amyloid beta-protein precursor promoter. Evidence for a role in transcriptional activation. *J. Biol. Chem.* 272, 33353–33359.
- Wang, Y., et al., 2018. The 3D genome browser: a web-based browser for visualizing 3D genome organization and long-range chromatin interactions. *Genome Biol.* 19.
- Wang, W., et al., 2021. Epigenetic treatment of behavioral and physiological deficits in a tauopathy mouse model. *Aging Cell* 20, e13456.
- Wang, Q., et al., 2022. Exploring Epigenomic datasets by ChIPseeker. *Curr. Protocol.* 2, e585.
- Williams, J.B., et al., 2021. Transcriptomic analysis of human brains with Alzheimer's disease reveals the altered expression of synaptic genes linked to cognitive deficits. *Brain Commun.* 3, fcab123.
- Williams, J.B., et al., 2023. Inhibition of histone methyltransferase Smdy3 rescues NMDAR and cognitive deficits in a tauopathy mouse model. *Nat. Commun.* 14, 91.
- Wilson 3rd, D.M., et al., 2023. Hallmarks of neurodegenerative diseases. *Cell*. 186, 693–714.
- Wingo, A.P., et al., 2019. Large-scale proteomic analysis of human brain identifies proteins associated with cognitive trajectory in advanced age. *Nat. Commun.* 10, 1619.
- Xie, Z., et al., 2007. Kalirin-7 controls activity-dependent structural and functional plasticity of dendritic spines. *Neuron*. 56, 640–656.
- Yang, J.H., et al., 2023. Loss of epigenetic information as a cause of mammalian aging. *Cell*. 186, 305–326.e27.
- Yu, G., et al., 2015. ChIPseeker: an R/Bioconductor package for ChIP peak annotation, comparison and visualization. *Bioinformatics*. 31, 2382–2383.
- Zhang, B., et al., 2013. Integrated systems approach identifies genetic nodes and networks in late-onset Alzheimer's disease. *Cell*. 153, 707–720.
- Zheng, Y., et al., 2019. Inhibition of EHMT1/2 rescues synaptic and cognitive functions for Alzheimer's disease. *Brain*. 142, 787–807.
- Zhou, Y., et al., 2019. Metascape provides a biologist-oriented resource for the analysis of systems-level datasets. *Nat. Commun.* 10.